



InSAR time series analysis of seasonal surface displacement dynamics on the Tibetan Plateau

5 Eike Reinosch¹, Johannes Buckel², Jie Dong³, Markus Gerke¹, Jussi Baade⁴, Björn Riedel¹

¹ Institute of Geodesy and Photogrammetry, Technische Universität Braunschweig, Braunschweig, Germany

² Institute of Geophysics and extraterrestrial Physics, Technische Universität Braunschweig, Braunschweig, Germany

10 ³ School of Remote Sensing and Information Engineering, Wuhan University, Wuhan, China

⁴ Department of Geography, Friedrich-Schiller-Universität Jena, Jena, Germany

Correspondence to: Eike Reinosch (e.reinosch@tu-braunschweig.de)

Abstract. Climate change and the associated rise in air temperature have affected the Tibetan Plateau to a significantly stronger degree than the global average over the past decades. This has caused deglaciation, permafrost degradation and increased precipitation, heavily changing the water balance of this region. Surface displacement processes are likely to change as the ground continues to warm up and as such it is vital to understand both seasonal and interannual processes dynamics. The Nam Co area is well suited to studying these processes via Interferometric Synthetic Aperture Radar (InSAR) time series analysis, due to its lack of higher vegetation and relatively thin snow cover. The short revisit time of the Sentinel-1 system further reduces the risk of temporal decorrelation, making it possible to produce surface displacement models with good spatial coverage. We created three different surface displacement models to study freeze-thaw processes, seasonal sliding and linear creep. Most slopes of the area are unstable, with velocities of 8 to 17 mm yr⁻¹, and some landforms reach velocities of up to 18 cm yr⁻¹. The monsoonal climate accelerates those movements during the summer months through high temperatures and heavy rainfall. The fastest moving landforms, some of which have been identified as rock glaciers, do not follow this seasonal pattern of accelerated velocity in summer, instead they follow a linear sliding pattern. It is unclear if this linearity is connected to the ice content in those landforms. Flat regions at Nam Co are mostly stable on a multiannual scale but some experience subsidence, which could be caused by permafrost degradation. We observe a very clear seasonal freeze-thaw cycle in the valleys, where thawing and subsequent freezing of the active layer cause a vertical oscillation of the ground of up to a few centimeters, especially near streams and other water bodies.

15
20
25
30



1 Introduction

35 The Tibetan Plateau (TP) has been the object of many studies focusing on climate change over the
past decades, especially since it has become known, that its temperature has risen significantly faster
than the global average with a rate of $0.025^{\circ}\text{C yr}^{-1}$ (Yao et al., 2000). This issue is exacerbated by the
importance of the TP as a source of fresh water for large parts of greater Asia (Messerli et al., 2004).
The TP is often referred to as the “Third Pole”, as it carries the largest volume of frozen fresh water
40 after the North- and South-Pole. The rising temperature, however, has led to deglaciation at rates of
over $0.2\% \text{ yr}^{-1}$ (Ye et al., 2017) and permafrost degradation (Wu et al., 2010) throughout the plateau,
increasing the river runoff by 5.5% (Yao et al., 2007). Glaciers and their retreat are very well
documented on the TP, as they can be assessed using optical satellite data with high accuracy (e.g.
Bolch et al., 2010). Permafrost features, such as rock-glaciers or buried ice lenses, are significantly
45 harder to quantify using optical remote sensing due to their debris cover. This has led to a severe lack
of inventories documenting these permafrost features, despite their importance as water storages
(Jones et al., 2019). Other studies have employed Interferometric Synthetic Aperture Radar (InSAR)
techniques to study permafrost features (e.g. Daout et al., 2017; Dini et al., 2019; Eriksen et al. 2017).
InSAR analysis is an active remote sensing technique, which exploits phase changes of backscattered
50 microwaves to determine relative surface displacements taking place between two or more
acquisition dates (Osmanoğlu et al., 2016). Both seasonal displacement processes, such as the
subsidence and subsequent uplift of thawing and freezing ground, and multiannual motion
processes, like the creep of periglacial landforms, can be studied. However, interpreting InSAR data
can be challenging and often a number of assumptions have to be made. InSAR models provide only
55 motion towards the satellite or away from it, not absolute ground displacement. It is therefore very
difficult to accurately assess ground motion, without making assumptions about its actual direction.
Unlike optical satellites, which observe the earth from a vertical Line-Of-Sight (LOS), SAR satellites
observe the earth at an angle. In the case of Sentinel-1 this angle varies between 33° and 43° from the
vertical (Yagüe-Martínez et al., 2016). SAR satellites are generally right-looking, meaning the
60 microwaves are emitted to the right of the satellite. Due to the polar orbit, this causes the
microwaves to be emitted in a near-east direction while the satellite is ascending and in a near-west
direction during descending data acquisitions.

The high elevation of the TP brings both advantages and disadvantages to InSAR application. High
altitudes can be problematic due to artifacts caused by atmospheric delay (Li et al., 2012), while the
65 lack of high and dense vegetation reduces the risk of decorrelation, which would otherwise lead to
poor coherence. Coherence is a measure of phase stability and is often used to represent the quality
of an interferogram and to determine which pixels will be processed further (Crosetto et al., 2016). A

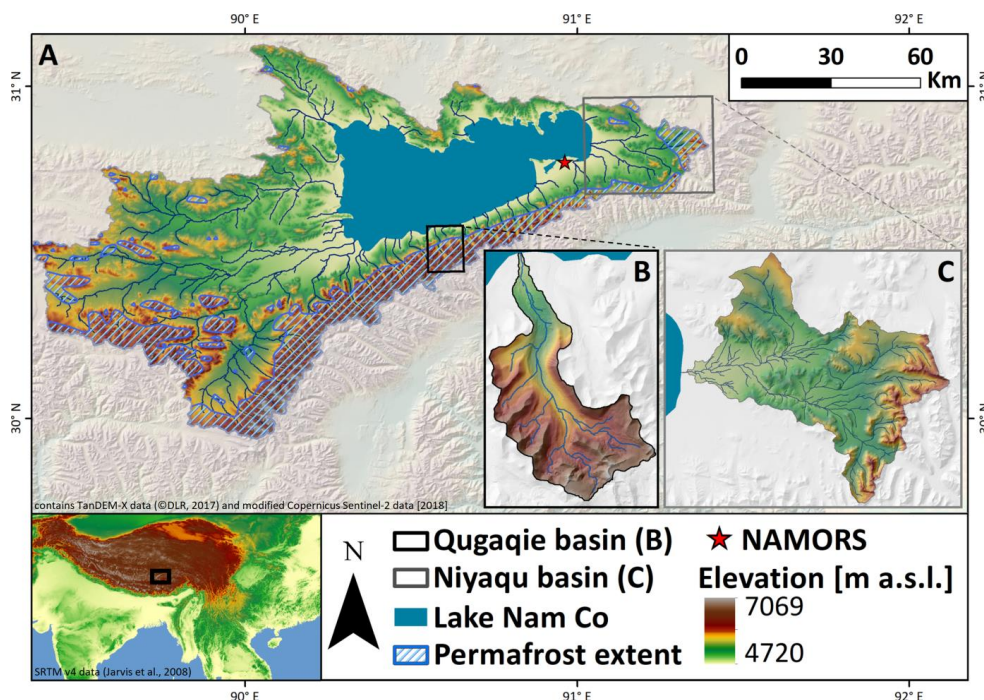


problem encountered by many studies investigating periglacial landscapes with InSAR techniques is heavy snow cover during the winter months (e.g. Eriksen et al., 2017), often leading to a complete
70 loss of coherence. This is not a problem in our study sites at Lake Nam Co. In fact, we found that coherence is highest in winter, which we attribute to a stable frozen ground without growing vegetation.

This paper identifies the various surface displacement processes taking place around Nam Co on the southern TP and evaluates their potential causes. It is vital to understand these displacement
75 patterns and to compare our results to similar studies, as the TP reacts heterogeneously to climate change. Some lakes on the TP show a rising lake level, while others show stable or even falling lake levels (Mügler et al., 2010; Jiang et al., 2017). By assessing land surface displacements processes at Nam Co, we gain further information about the local situation, which allows us to set this region into a more accurate context compared to other regions of the TP. To that end we developed multiple
80 surface displacement models, analyzing geomorphological processes in the valleys and on the mountain slopes on both a seasonal and a multiannual scale. Furthermore we evaluate our hypothesis to predict if the creep of a periglacial landform is driven by its high ice content by differentiating between linear and seasonal motion patterns. This hypothesis is based on the assumption, that a high ice content within the landform could facilitate significant creep throughout
85 the year, leading to a linear motion pattern, while landforms without ice show no motion during periods when the ground is frozen, hence following a seasonal motion pattern.

2 Study Area

The Nam Co is the second largest lake of the TP (Zhou et al., 2013), with a catchment covering an
90 area of 10,789 km², 2018 km² of which is the lake's own surface area (Zhang et al., 2017). The proximity to Lhasa, its accessibility and the presence of the scientific research station NAMORS (Fig. 1), have made it a prime location to study the effects of climate change on the TP. The current lake level lies at 4726 m a.s.l. (Jiang et al., 2017) but it has featured a rising trend of approximately 0.3 m yr⁻¹ over the past decades (Kropáček et al., 2012; Lei et al., 2013). To the north and west the
95 endorheic catchment borders on the catchments of smaller lakes, such as Renco and Bamu Co. The eastern and southern borders of the catchment are defined by the eastern and western Nyainqêntanglha mountain ranges respectively. They feature elevations of up to 7162 m a.s.l. and are partially considered to be periglacial area (Keil et al., 2010; Li et al., 2014), while their highest reaches are glaciated (Bolch et al., 2010).



100

Fig. 1: Overview map of the Nam Co catchment (A) including the locations of the NAMORS research station and the two main study areas: Qugaqie basin (B) and Niyaqu basin (C). Elevation data based is on SRTM v4 (Jarvis et al., 2008) and TanDEM-X 0.4'' DEM (©DLR, 2017). Permafrost extent according to Zou et al. (2017) and lake extent based on the Normalized Difference Water Index (NDWI) of Sentinel-2 optical imagery (©Copernicus Sentinel data 2018, processed by ESA).

105

The climate at the Nam Co is dominated by the Indian Monsoon in summer and the Westerlies in winter (Yao et al., 2013). The former brings warm moist air from the south, providing 250 to 450 mm of rainfall from June to September and accounting for approximately 80% of the annual precipitation (NAMORS, 2018; see Fig. 1A). The Westerlies maintain semi-arid to arid conditions during the rest of the year. The snow cover is relatively sparse in winter, due to low precipitation outside of the monsoon season. The vegetation consists primarily of alpine steppe (Li, 2018), with higher vegetation, such as shrubs and trees, being almost completely absent. The sparse snow cover and the lack of vegetation make this region a prime study site for periglacial processes using InSAR technology. Wang et al. (2017) used a combination of InSAR and optical satellite data to map rock-glaciers in the northern Tien Shan of China, where the winters are similarly dry. The risk of temporal decorrelation, i.e. the loss of data coverage due to a strong change of physical surface characteristics, is significantly lower than in other regions where such processes may be studied, such as Norway

110

115



(Eriksen et al., 2017) or the Sierra Nevada in the USA (Liu et al., 2013). These regions feature
120 significant snow cover during long periods of the year, making consistent coverage of fast-moving
structures, like rock-glaciers, difficult. This is especially a problem for satellites with the shorter X-
band (2-4 cm) or C-band (4-8 cm) wavelengths, like TerraSAR-X (3.1 cm) and Sentinel-1 (5.6 cm), as
they are more susceptible to temporal decorrelation (Crosetto et al., 2016) compared to systems
with a longer wavelength such as L-Band (15-30 cm).

125 The two areas of interest for this study are the Qugaqie basin (58 km²) within the western
Nyainqêntanglha mountain range, south of the Nam Co and the Niyaqu basin (409 km²) at the
eastern Nyainqêntanglha mountain range, on the eastern shore of the lake (Fig. 1). Those sub-
catchments were chosen, to represent different levels of glacial impact and the predominant
landscapes and their related surface motion processes at Nam Co. The Niyaqu basin represents the
130 majority of Nam Co's catchment with extensive alpine steppe vegetation and wetlands surrounded
by hills with little exposed bedrock in the lower regions. The global permafrost map of Zou et al.
(2017) suggests that periglacial processes are limited to the higher reaches of the sub-catchment, at
the eastern Nyainqêntanglha mountain range. The Qugaqie basin represents the periglacial
landscape of the western Nyainqêntanglha mountain range. 60 % of its area are considered
135 periglacial landforms (Li et al., 2014), some of which are still active in the higher reaches of the
catchment due to their potential ice content, such as rock glaciers. Rock glaciers are steadily creeping
ice-rich debris on mountainous slopes associated with permafrost (Haeberli et al., 2006). Other
landforms were accumulated through fluvial, glacio-fluvial, glacial and aeolian processes (Keil et al.,
2010). The vegetation cover is similar but with more areas of exposed glacial valley fill and bedrock
140 interspersed in between the vegetated areas. Both the valleys and the slopes are covered by
unconsolidated material, mostly coarse gravel and boulders, with some slopes being virtually free of
soil and vegetation. The main river is fed by hanging valleys, some containing glaciers, as well as the
two main glaciers Zhadang and Genpu to the south. The glaciers cover 8.4 % of the basin's surface
area and account for 15 % of its runoff in summer (Li et al., 2014). Two automated weather station
145 and a rain gauge were operated near the ablation zone of the Zhadang Glacier between 2005 and
2010. Daily temperature averages range from approximately -15°C in winter to 3°C in summer in the
Qugaqie basin and -10°C to 10°C in the Niyaqu basin (NAMORS 2018; Zhang et al., 2013)



3 Data

We use exclusively Sentinel-1 Level-1 single look complex data for all InSAR analysis, both from ascending and descending orbits from the interferometric wide swath mode with a ground resolution of 20 m azimuth and 5 m in range direction (ESA, 2012). Sentinel-1a has been acquiring data since
155 October 2014 and Sentinel-1b since September 2016. We found early data acquisitions of Sentinel-1a to be very unreliable over the Qugaqie basin, which is why we decided to start our time series analysis of this area in May and November 2015 for ascending and descending acquisitions respectively. Early data over the Niyaqu basin is more stable, here we start our time series analysis in December 2014 for both ascending and descending acquisitions. The latest data acquisitions included
160 in the analysis are from November and December 2018. Sentinel-1b data is not available for this region, except for a 3 months period at the end of 2016 in descending orbit. More detailed information about the number of acquisitions and interferograms is shown in Table 1. We carefully analyzed all individual interferograms and excluded those with long temporal or geometric baselines, unwrapping errors and overall low coherence and therefore poor spatial coverage. All topographic
165 analysis and processing, including the removal of the topographic phase from the InSAR data was conducted, using the 0.4 arc sec, equal to 12 m at the equator, resolution TanDEM-X DEM (©DLR, 2017). This new and truly global DEM has been acquired in the years 2010 to 2015 using single-pass X-Band SAR interferometry (Zink et al. 2014) and finally released by German Aerospace Agency in 2017. On the global scale the DEM features an absolute error at 90% confidence level of < 2 m
170 (Wessel et al. 2018). In steep terrain accuracy is ensured by multiple data takes in ascending and descending orbits with varying incidence angles to prevent radar shadows and overlay. In the Niyaqu basin, the number of acquisitions per pixel ranges from 5 to 8, with the majority representing average height estimates based on 6 acquisitions. Here, the mean 1 σ height error is 0.30 m. In the steeper Qugaqie basin the number of acquisitions ranges from 8 to 12, with the majority at 9
175 acquisitions. Here the mean of the 1 σ height error is 0.35 m.

Table 1: Sentinel-1 data used for the time series analysis of both study areas.

Area of interest	orbit	Acquisition period	Acquisitions / interferograms
Niyaqu basin	ascending, track 41	2014-12-31 to 2018-12-22	79 / 244
Niyaqu basin	descending, track 150	2014-12-14 to 2018-11-11	72 / 227
Qugaqie basin	ascending, track 41	2015-06-05 to 2018-12-22	74 / 278
Qugaqie basin	descending, track 150	2015-11-15 to 2018-12-29	63 / 257



4 Methods

4.1 ISBAS Processing

180 There are many different InSAR techniques capable of time series analysis to determine a region's
surface displacement over time. We chose a modified version of the Small Baseline Subset (SBAS)
method (Berardino et al., 2002), which we performed with the ENVI SarScape software (©Sarmap
SA, 2001-2019). The SBAS method generates interferograms between SAR acquisitions with a short
temporal baseline, meaning the time between the acquisitions was short, and stacks them to
185 estimate -displacement and velocity over a longer time period. Interferograms are a spatial
representation of the phase difference of two SAR acquisitions and can be used to determine the
relative surface displacement between them. This modified SBAS approach, referred to as
Intermittent SBAS (ISBAS) (Sowter et al., 2013; Batson et al., 2015), produces a significantly improved
spatial coverage by allowing limited interpolation of temporal gaps for areas, where the coherence is
190 intermittently below the chosen threshold. This reduces one of the downsides of the original SBAS
algorithm, where partially vegetated areas can often not be processed, due to only producing good
coherence for some interferograms but not all. We chose a coherence threshold of 0.3 for our
velocity models with an intermittent value of 0.75 and therefore 75 % of the interferograms need to
produce a coherence of at least 0.3 to be considered during unwrapping. These parameters are
195 similar to those used by Sowter et al. (2013) and Bateson et al. (2015) and produce an acceptable
compromise of good spatial coverage, while excluding most unreliable data from the unwrapping
process. We found that the seasonal freeze-thaw signal is most prominent near water bodies, where
coherence is very low. We therefore decided to use a very low coherence threshold of 0.1 to increase
spatial coverage in those areas, only for the analysis of the freeze-thaw cycle for our Freeze-Thaw
200 Model (FTM). Both the Multiannual Velocity Model (MVM) and the Seasonal Sliding Model (SSM) use
a threshold of 0.3. The models are explained in detail in the Sections 4.3 to 4.5 and a summary may
be found in Table 2.

The topographic phase was removed from the interferograms with the TanDEM-X 0.4 arcsec
resolution DEM (Wessel et al., 2018) and the orbital phase was corrected via a polynomial function
205 prior to unwrapping. We used a linear model for all processing and applied a short atmospheric high
pass filter of only 100 days, to preserve the seasonal signal for our time series analysis, and a low
pass filter of 1200 m.

After performing the ISBAS processing chain, flat areas within Qugaqie basin retained a relatively
strong shift of up to 9 mm yr⁻¹ and 13 mm yr⁻¹ in ascending and descending datasets respectively. Due
210 to the respective correlations with a R² of 0.12 and 0.38 between this shift and elevation, we



concluded that this signal is likely connected to an atmospheric phase delay rather than actual surface motion. We therefore performed a linear spatial trend correction to remove this shift from both ascending and descending datasets. After these corrections we observe east-west velocities of $-0.2 \pm 2.2 \text{ mm yr}^{-1}$ and $-0.9 \pm 2.4 \text{ mm yr}^{-1}$ in likely stable areas in Niyaqu and Qugaqie basin respectively.

215 The error range of the slope projection can be up to 5 times as high for areas with a very strong coefficient caused by a large difference between the projection direction and the LOS of the satellite.

4.2 Selection of reference areas

InSAR products are relative not only to the LOS of the satellite but also to the chosen reference points or areas. It is necessary to select at least one reference to perform the unwrapping process during the InSAR processing chain. Stable GNSS stations are preferred reference points but there are no permanent GNSS stations installed near the study areas. Therefore it is necessary to select the reference areas carefully to avoid introducing a false signal into the surface displacement models. The parameters by which those reference areas were chosen are:

- 225 1.) Only points located at high elevation, far away from the valley floor were considered. The annual freeze-thaw cycle, and the corresponding uplift and subsidence of the ground, is very strongly represented in the highly moisturized ground of the valley floor. Choosing reference points in this environment would remove this annual ground oscillation from the dataset in the valley floor and create an artificial and opposite oscillation pattern in other areas. The
- 230 ridges of the Nyainqêntanglha mountain ranges on the other hand feature barely any soil and contain significantly less moisture. Freezing and thawing of the ground should therefore cause a less pronounced oscillation.
- 2.) The chosen reference points must not have any significant velocity by themselves, as this would shift the entire velocity model. We compared the results of different reference points
- 235 in areas where we expect little multiannual velocity and discarded those that caused a significant shift. As reference areas we chose regions with a low slope, good coherence and no obvious deformation structures, and assume them to be stable in time.
- 3.) Ideally the reference points are located on unmoving bedrock. Bedrock has a much smaller porosity than loose sediment or soil and is therefore less prone to strong oscillations forced
- 240 by freezing and thawing of pore fluid.
- 4.) The reference points must be at locations which are represented clearly in 100 % of all interferograms generated during the SBAS processing chain, to ensure that the displacement of all interferograms can be correctly determined relative to those points.



245 Despite our careful selection of reference points, we cannot be certain, that those areas are in fact
stable throughout the entire data acquisition period. We chose to use multiple reference points
instead of a single point to produce the surface velocity models. This was done to prevent a single,
potentially poorly selected, reference point from invalidating the entire dataset by introducing either
a multiannual shift or seasonal signal. The areas of partially exposed bedrock and the mountainous
250 terrain of the Qugaqie basin made the selection of reference points significantly easier compared to
the Niyaqu basin, where exposed bedrock is rare. Selecting only points positioned at these optimal
locations left us with none near the center of the basins or the lake shore. This caused LOS shifts on a
millimeter scale in presumably stable flat areas, if they were far away from the reference points. We
therefore increased the number of reference points to 90 and 51 in the Qugaqie basin and 92 and 61
in the Niyaqu basin for ascending and descending acquisitions respectively. The number of reference
255 areas varies between ascending and descending acquisitions, due to differences in coherence, but we
chose the same reference areas whenever possible.

4.3 Multiannual Velocity Model (MVM)

260 This model portrays the mean annual surface velocity, with different methods applied to regions with
a slope $>10^\circ$ and with a slope $<10^\circ$. The original ISBAS processing chain (Sect. 4.1) is the same but we
applied different methods thereafter to project the LOS results into a more meaningful direction. For
areas with a slope $<10^\circ$ we assumed, that displacement would occur mainly in a vertical direction, as
the slope would be too small to facilitate significant sliding or creep in most cases (Daanen et al.,
2012) and no tectonic processes, which could produce lateral motion, have been documented for
265 this area. To determine the vertical velocity, we performed a decomposition of ascending and
descending time series data. For this process we assume the north-south component of the ground
motion to be zero, which allows us to determine the vertical and east-west component (Eriksen et
al., 2017). The vertical component represents our expected surface velocity for flat areas, while the
east-west component can be used to assess the error range of the velocity model.

270 The decomposition method works well for flat regions and slopes with an east or west aspect but
does not produce useful data for slopes with a north or south aspect. SAR satellites are quite
sensitive to both east-west and vertical surface motion but very insensitive to motion with a strong
north or south component. This is problematic when studying lateral sliding and creeping processes,
as the velocity of areas moving in a northern or southern direction will be either severely
275 underestimated or completely overlooked. We therefore employed a different method for slopes.
Areas with a slope $>10^\circ$ were projected in the direction of the steepest slope (after Notti et al., 2014),



as most surface displacement is assumed to be caused by sliding processes transporting material parallel to the slope (Fig. 3). We made an exception for areas with a large east-west velocity, as one of our study areas features a periglacial setting with landforms such as rock glaciers, which may extend into flatter areas. Those areas were projected in a downslope direction, even on slopes $<10^\circ$. Our method (after Notti et al., 2014) originated from landslide studies, to produce a more accurate result for a process, where the direction of the moving structure is either known or can be assumed with reasonable certainty. To estimate the downslope velocity, we calculate a coefficient, with values between 0.2 and 1, based on the LOS of the satellite and the aspect and slope of the surface area. The larger the difference between the LOS vector and the vector representing the assumed motion direction, in this case downslope, the smaller and therefore stronger the coefficient becomes. We excluded data points with a strong coefficient if a slope has a strong coefficient in only one LOS but not the other, as a strong coefficient is associated with a larger uncertainty. The maximum strength of this coefficient is set to 0.2 to avoid producing unrealistically large results caused by a coefficient close to zero. We used smoothed version of the TanDEM-X DEM (90 x 90 m moving mean) to determine the motion direction. We assume that structures such as rock glaciers and landslides move a larger amount of sediment in a similar direction. It is important to note, that by projecting LOS velocities along the steepest slope, we not only assume the direction vector, but we also simplify the mechanics to that of a planar slide. In doing so we assume that neither rotational nor compressing processes are involved. This is an obviously unrealistic but necessary simplification, which leads to an overestimation of the downslope velocity.

300

305



Table 2: Overview of the 3 surface displacement models with information about their purposes, displacement patterns and their connections to geomorphological und geological parameters.

Modeltype	FTM (Freeze-Thaw Model)	SSM (Seasonal Sliding Model)	MSM (Multiannual Velocity Model)
Purpose	Provide information about soil freezing properties	Differentiate between seasonal sliding and linear creep	Identify sediment accumulation and permafrost related processes
Min. Coherence	0.1	0.3	0.3
Displacement type	Seasonal vertical displacement	Seasonal displacement along the slope	Multiannual linear velocity along the slope
Slope	Mostly <10°	>10°	<10°: vertical velocity >10°: along slope velocity
Material	Mainly soil	Regolith, debris and ice	Soil, regolith, till, debris and ice
Related Geomorphological processes	Freeze-thaw cycles connected to cryoturbation	Solifluction and gelifluction on seasonally frozen slopes	Permafrost creep
Associated Landform	Hummocky terrain	Debris slopes and lobates	Rockglaciers, protalus ramparts and moraines

310

4.4 Freeze-thaw model (FTM)

Prior to analyzing the freeze-thaw amplitude, we projected the LOS displacements from both ascending and descending datasets to vertical displacement. We then removed the linear multiannual trend from the datasets to isolate the seasonal signal. A sum of sine function was estimated for each individual time series. For the amplitude estimation in the Qugaqie basin we used a function with two sine terms and for Niyaqu basin a function with three terms. We identified the sine term representing the annual signal and discarded the other terms. To qualify for further analysis, a time series must produce an annual freeze-thaw amplitude of larger than 3 mm, with a confidence of R^2 larger than 0.5 and a period of 350 to 380 days. Ascending and descending datasets were interpolated to produce mean amplitude results with a ground resolution of 15 x 15 m.

315

320



4.5 Seasonal Sliding Model (SSM)

The average seasonal velocities represent the median summer and median winter velocities over the entire time series. We divided the median summer velocity by the median winter velocity to produce the seasonal sliding coefficient, which represents how fast a surface is moving in summer compared to winter. Our multiannual velocity models feature a precision of around 2 mm yr^{-1} . Time series with median seasonal velocities within the $\pm 2 \text{ mm}$ error range were set to either -2 or 2 mm , to avoid artificially large values when calculating the seasonal sliding coefficient with median seasonal velocities close to 0.

330 5 Results

In total we produced three different types of surface displacement models for the Niyagu and the Qugaqie basin: The Multiannual Velocity Model (MVM), the Freeze-Thaw Model (FTM) and the Seasonal Sliding Model (SSM). The MVM portrays the mean surface velocity from 2015 to 2018. The FTM aims to isolate the seasonal vertical displacement caused by thawing of the active layer in spring followed by subsequent freezing of the active layer in autumn. The SSM was created to differentiate between slopes where sliding takes place primarily from spring to autumn and areas where sliding takes place throughout the year at a linear rate.

5.1 MVM: Linear surface velocity

340 For the MVM, we assumed that displacement occurring in areas with slopes $<10^\circ$ are predominantly vertical in direction, as the low slope is insufficient to produce significant lateral velocity. Daanen et al. (2012) observed, that slopes $<10^\circ$ were unable to support permafrost creep in Alaska. Their findings are corroborated by the east-west velocity produced by our decomposition of ascending and descending data. For the slopes of $0 - 5^\circ$, $5 - 10^\circ$ and $10 - 15^\circ$ we observe mean east-west velocities of $-0.1 \pm 3.0 \text{ mm yr}^{-1}$, $-0.6 \pm 2.9 \text{ mm yr}^{-1}$ and $-0.6 \pm 5.0 \text{ mm yr}^{-1}$. The jump in error range from the $5 - 10^\circ$ group to the $10 - 15^\circ$ from $\pm 3 \text{ mm yr}^{-1}$ to $\pm 5.0 \text{ mm yr}^{-1}$ suggests that we observe significantly more lateral motion in the latter group. This makes the 10° mark a good threshold between the vertical and the downslope projections. For areas with a slope $>10^\circ$ we assumed that the displacement would occur along the steepest slope, driven by gravitational pull (Haeberli et al., 2006) and facilitated by the unconsolidated material and lack of deep-rooted vegetation (Li et al., 2014).

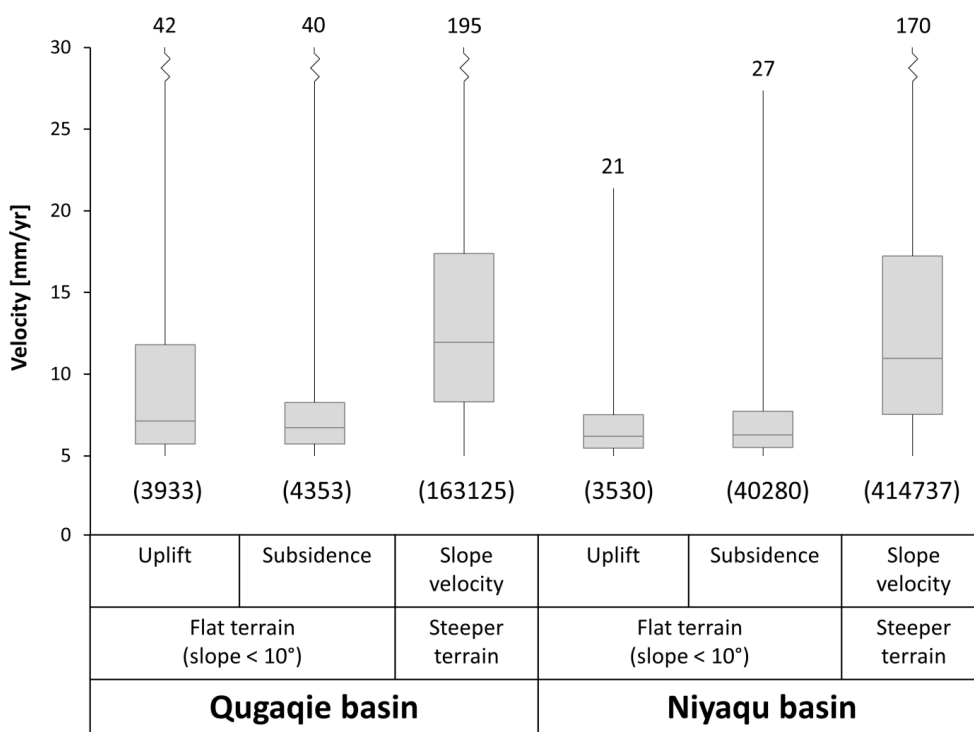


Fig. 2: Distribution of the mean velocity results for unstable flat and steep terrain for the MSV in both study areas. All surface motion in flat areas (slope <10°) was projected into vertical direction (uplift and subsidence) and motion in steeper areas was projected along the direction of the slope. The maximum values are shown above the respective plots and the amount of data points included in each plot is shown in parenthesis below them. Areas with velocities <5 mm yr⁻¹ are considered stable and are not shown here.

Spatial data gaps in our InSAR models are caused by layover and shadow effects in mountainous regions or where the coherence was lost due to streams, vegetation, rock falls and glaciers. These data gaps make up 34.7 % in flat and 31.4 % in steep areas within the Qugaqie basin and 30.5 % and 36.0 % in the Niyaqu basin. The decomposition of ascending and descending datasets of areas with a slope <10° shows that both basins are relatively stable in flat terrain on a multiannual scale. 53.3 % of the area in the Qugaqie basin and 64.4 % in Niyaqu basin fall within the ±5 mm yr⁻¹ velocity group in both vertical and east-west directions. We consider these areas to be stable. In the Quagqie basin 3.3 % of flat areas experience uplift, primarily near the main stream, while 2.8 % of flat areas are subsiding. In the Niyaqu basin 0.2 % of flat areas experience uplift and 2.7 % experience subsidence.



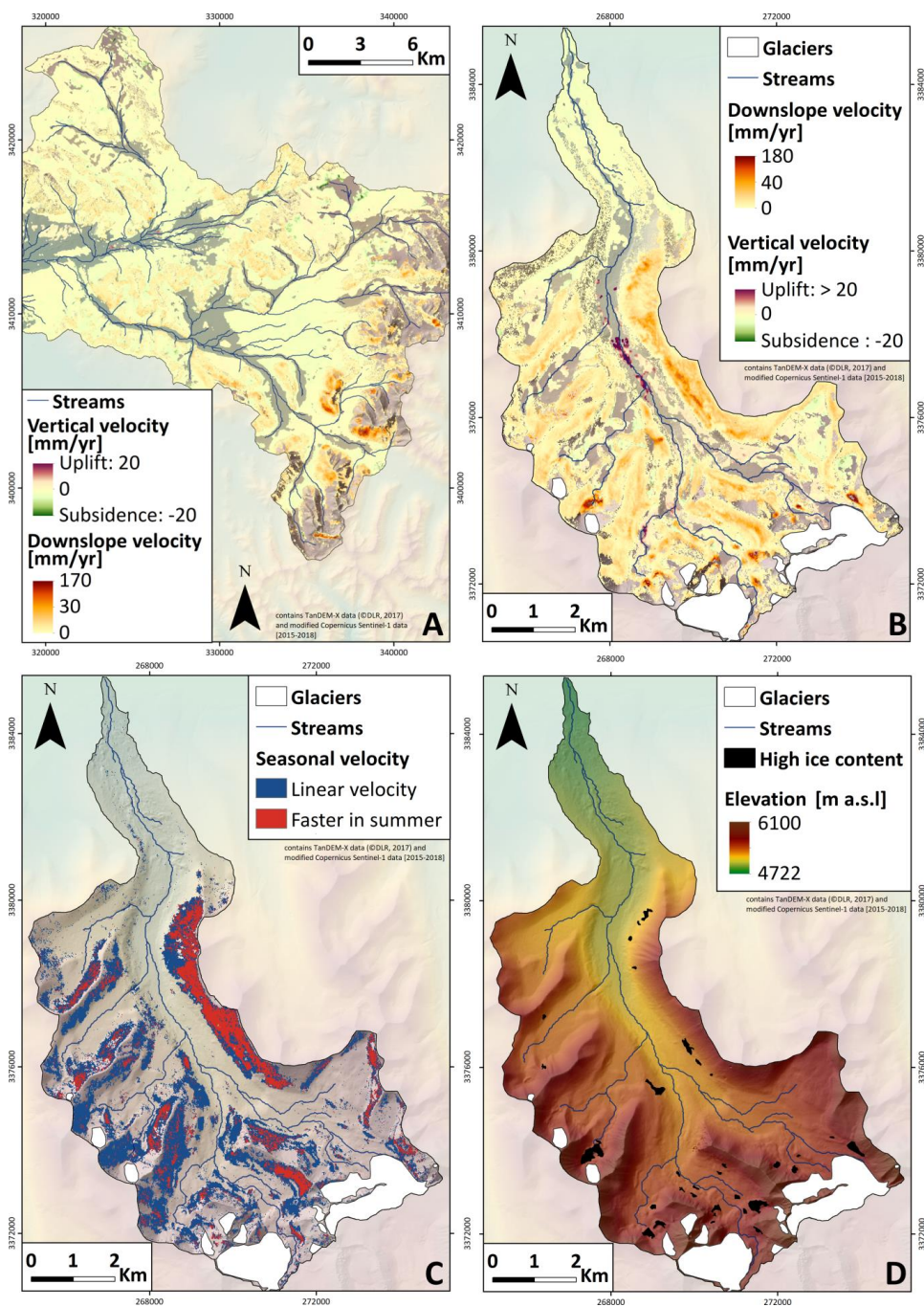
The remaining flat areas, 5.8 % in the Quagaqie and 2.1 % in the Niyaqu basin, experience minor lateral motion.

370 **Table 3:** Quantitative summary of our spatial data coverage of the MVM in both study areas. The
 shown values represent the percentages compared to all flat or steep areas in the respective study
 area. Incoherent areas display a mean coherence of <0.3 . Stable areas move with $<5 \text{ mm yr}^{-1}$ in all
 directions, unstable flat areas uplift / subside / move laterally at $>5 \text{ mm yr}^{-1}$, steep unstable areas
 move at $>5 \text{ mm yr}^{-1}$ downslope and very unstable terrain moves at $>30 \text{ mm yr}^{-1}$ into the same
 375 directions.

	Slope	Incoherent	Stable	Unstable	Very unstable
Quagaqie basin	flat ($<10^\circ\text{C}$)	34.7	53.3	3.3/2.8/5.8	0.1
	steep ($>10^\circ\text{C}$)	31.4	20.9	44.9	2.8
Niyaqu basin	flat ($<10^\circ\text{C}$)	30.5	64.4	0.2/2.7/2.1	0.0
	steep ($>10^\circ\text{C}$)	36.0	21.1	39.7	3.1

Steeper areas, with a slope $>10^\circ$, are significantly more unstable in both study areas. In the Quagaqie basin only 20.9 % of slopes are stable, with 2.8 % being very unstable with velocities $>30 \text{ mm yr}^{-1}$. In the Niyaqu basin 21.1 % of sloped areas are stable and 3.1 % are very unstable. A summary of the spatial data coverage is shown in Table 3. Most of the low coherence areas would likely be considered unstable as well and would therefore increase the percentage of unstable and very unstable areas. A distribution of the absolute surface velocity results in different regions is shown in Figure 2.

380



385 **Fig. 3:** Surface displacement models of the relevant parts of the Niyaqu and Qugaqie basins based on
 Sentinel-1 data (modified Copernicus Sentinel-1 data [2015-2018]) over TanDEM-X DEM (©DLR,
 2017). **A/B:** MSM of Niyaqu/Qugaqie basin, where areas with a slope <10° show vertical velocity and



390 *steeper slopes show the surface velocity projected along the steepest slope. C: SSM of Qugaqie basin displaying the spatial distribution of linearly moving slopes and those with a more than 50 % faster velocity in summer as compared to winter. Only areas with a slope >10° and a slope velocity >10 mm yr⁻¹ are shown. D: Spatial distribution of clusters where we assume a high ice content based on a high slope velocity with a linear pattern.*

The coherence in both basins is much reduced in valley areas. Streams and other water bodies
395 inundate the soil with moisture, creating large changes in microwave backscatter properties depending on the season. More extensive vegetation near the valley bottom further reduces the coherence there. The coherence is especially low in those areas during spring and the summer monsoon period, when the ground thaws, the surface is inundated by rain water and biomass production increases. This causes an overall drop in spatial data coverage in valleys, as many
400 resolution cells exhibit coherence values below the threshold.

5.2 FTM: Freeze-thaw amplitude

The vertical oscillation of the ground due to freezing and thawing of the soil is strongest at the valley bottom, especially near streams, lakes, ponds and, in the case of Qugaqie basin, glaciers. In these
405 areas the amplitude of this oscillation can reach up to 19 mm (Qugaqie basin, Fig. 5C) or even 27 mm (Niyaqu basin, Fig. 5A). The day of maximum subsidence (DMS) is the day in summer during which the soil has thawed to its maximum extent before beginning to freeze again in autumn (Fig. 5 B/D). In the Qugaqie basin the median DMS is on July 12 and in the Niyaqu basin it is on August 24 (Fig. 4). Most areas with freeze-thaw amplitudes of <7 mm reach their day of maximum subsidence in July to
410 August in the Niyaqu basin and May to July in the Qugaqie basin, while areas with larger amplitudes tend to reach theirs in September to October (Fig. 5E/F). This trend is more pronounced in the Qugaqie basin. We compared the DMS results of ascending and descending datasets and noticed that in both basins the mean DMS of the descending dataset occurs earlier. In the Niyaqu basin the difference between ascending and descending DMS is 27 days and in the Qugaqie basin 11 days. For
415 this comparison we only took areas into account with a large density of both ascending and descending data points.

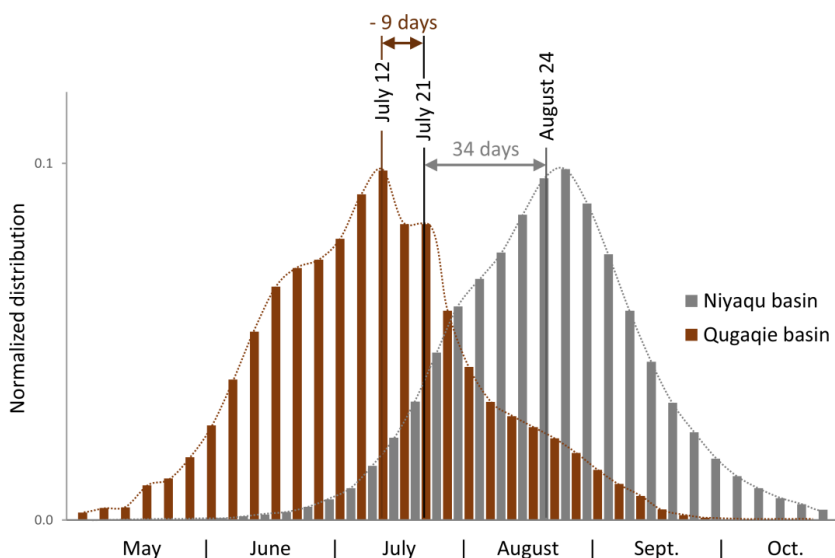
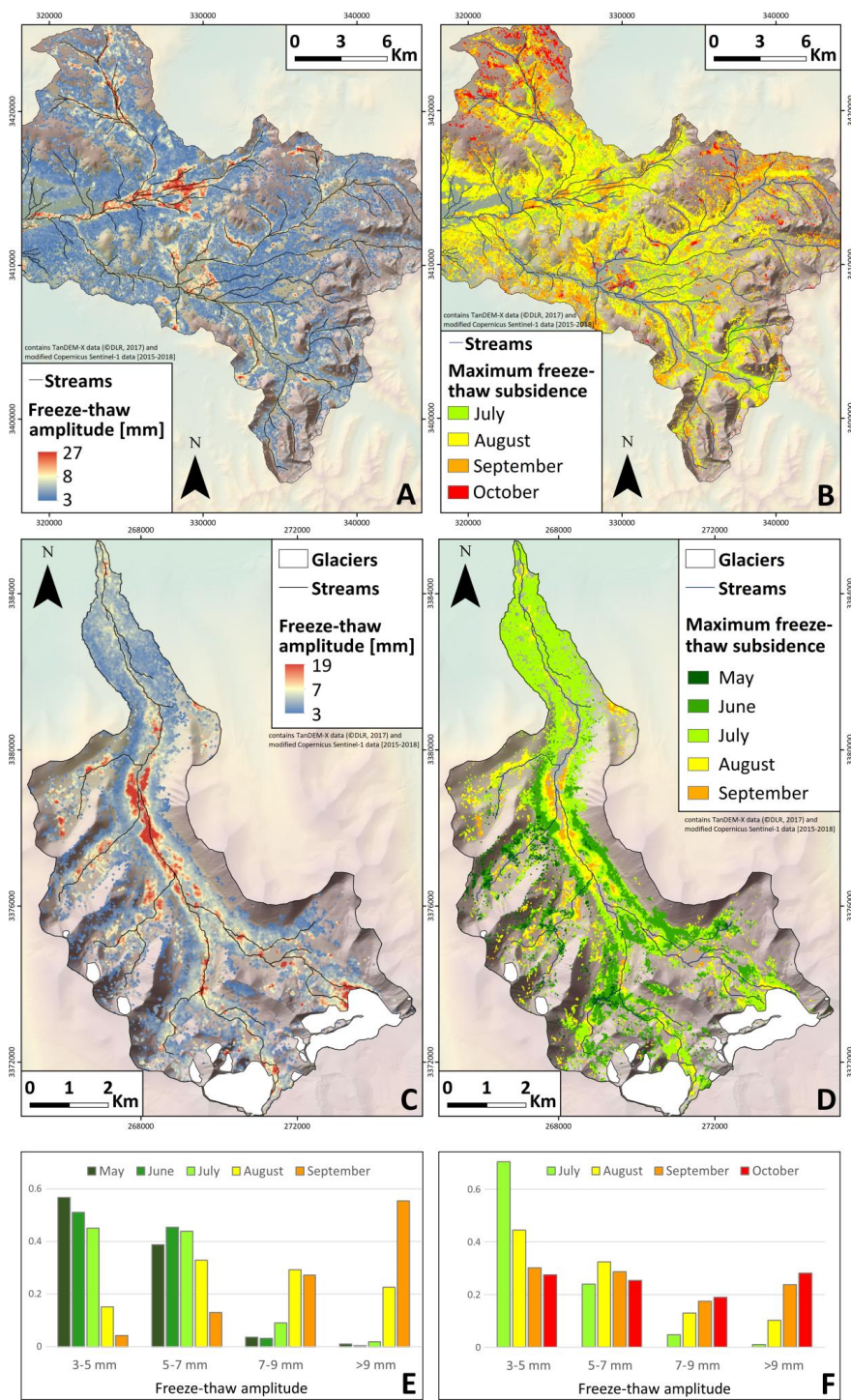


Fig. 4: Normalized distribution of the thaw-induced day of maximum subsidence (DMS) in the Niyaqu (grey) and the Qugaqie (brown) basins and their respective median values on August 24 and July 12.

420 The lag time between those median values and the day of the mean maximum air temperature are also shown. The mean air temperature peak occurs on July 21 (NAMORS, 2018), resulting in a lag time of 34 days in the Niyaqu basin and no lag time in the Qugaqie basin, as there the median DMS occurs 9 days prior to the mean air temperature peak.

425 Other studies (Li et al., 2015; Daout et al., 2017) have stated that there is often a significant lag time between the day of maximum air temperature and the DMS. According to the weather data from the NAMORS research station, the air temperature has a mean peak on July 21±1 day from 2010 to 2017. Data from the weather station at the Zhadang glacier (Zhang et al., 2013) shows this mean peak on July 27±5 days for 2010 to 2011. Due to the short data acquisition period of the data from this
430 weather station, we chose the more robust data set of the NAMORS for both study areas. This produces a lag time of approximately 34 days for Niyaqu basin (Fig. 4, grey), while in the Qugaqie basin the median DMS occurs 9 days ahead of its temperature peak (Fig. 4, brown). We used this lag time to determine the active layer thickness (ALT) by assuming the heat transfer to be one-dimensional and the soil to be homogeneous. Our chosen thermal diffusivity is $4 \times 10^{-7} \text{ m}^2/\text{s}$, based on
435 the mean value for frozen soil after Wang et al. (2005), and we followed the heat transfer model of Li et al. (2015). The resulting ALT is $1.3 \pm 0.7 \text{ m}$ for Niyaqu basin. We did not determine the ALT for Qugaqie basin, as we do not observe a lag time here and the system is therefore likely too complex for this simplified approach.





440 **Fig. 5:** Seasonal freezing and thawing parameters (modified Copernicus Sentinel-1 data [2015-2018])
over TanDEM-X DEM (©DLR, 2017). Spatial variations of the mean amplitude (**A/C**) and the day of
maximum subsidence (**B/D**) of the FTM within the Niyaqu/Qugaqie basin. **E/F:** Normalized
distribution of the months in which the freeze-thaw cycle reaches their maximum subsidence split up
into 4 groups according to their amplitude for the Niyaqu/Qugaqie basin.

445

5.3 SSM: Seasonally sliding slopes

We identified two distinct seasons, the wet monsoon season in summer and the dry winter season,
which have a significant impact on the displacement data. The former season causes more
pronounced ground sliding on many slopes, while the latter arrests most sliding processes. In Niyaqu
450 basin the displacement pattern of the summer period lasts from May to September and in Qugaqie
basin from June to October. The winter displacement patterns last from November to March and
from December to April respectively. We compared the median summer velocities to the median
winter velocities of each time series over the entire time-period. Most debris covered slopes in both
basins slide significantly faster during the summer months and some of them, especially in the
455 Qugaqie basin, stop their motion altogether in winter (Fig. 4 C).

In Qugaqie basin some of the fastest moving structures creep at a linear rate as opposed to the
strong seasonality of most slopes. Their velocity changes very little between summer and winter and
is generally between 30 to 180 mm yr⁻¹. We performed a cluster analysis of these structures to
identify their distribution throughout the valley and noticed that some of them correspond to
460 periglacial features we identified from optical satellite imagery, field observations and topographic
analysis. The motion of these permafrost related structures, such as rock-glaciers and protalus
ramparts, is driven by an ice matrix in between unconsolidated debris material (Haerberli et al., 2006).

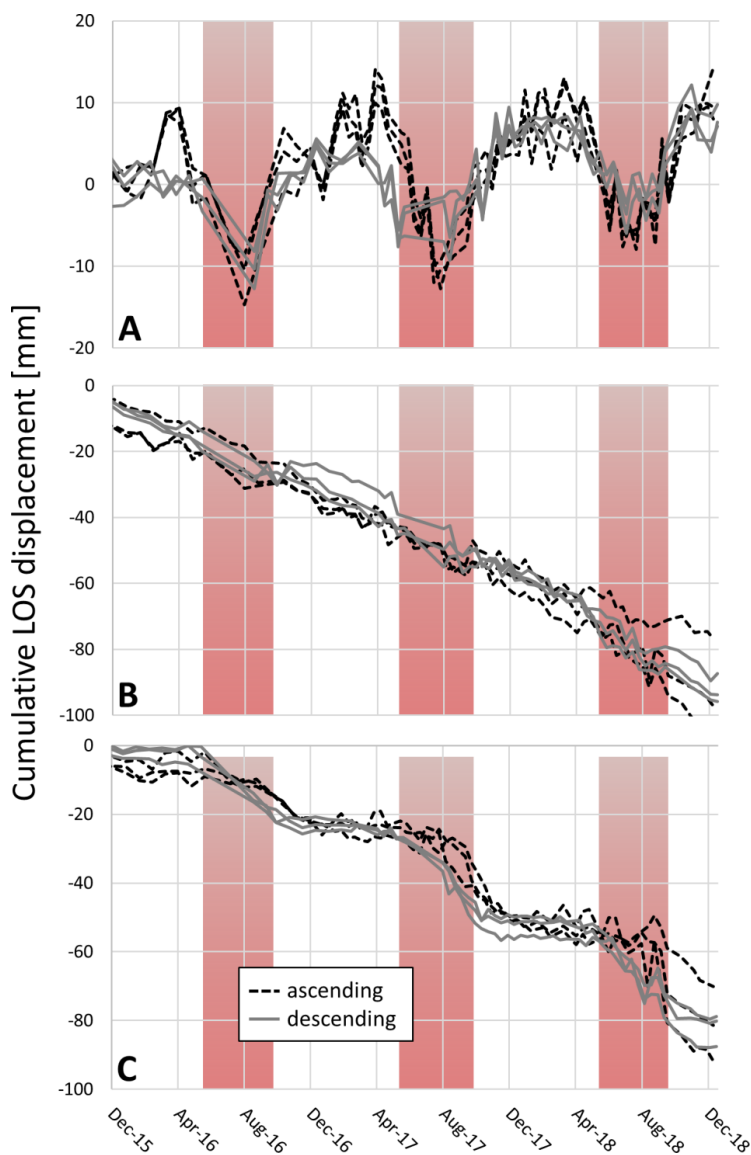


Fig. 6: Cumulative LOS displacement of both ascending (black dashed) and descending (grey) data of
465 various areas throughout Qugaqie basin highlighting the three seasonal patterns. The months with
the strongest monsoon activity (June to September) are shown with a red background. **A:** Seasonal
freeze-thaw cycle of the FTM near the stream of the main valley. **B:** Linear displacement patterns of
various structures classified as potentially containing a large amount of ice (blue areas in Fig. 3C). **C:**
Seasonal displacement patterns of various slopes highlighted by the SSM with large displacements in
470 summer and comparatively minor displacements in winter (red areas in Fig. 3C).



6 Discussion

Zhao et al. (2016) demonstrated, that using a linear model to process regions with cyclical freeze-thaw mechanisms leads to an overestimation of the displacement signal. We could not confirm their findings in our study areas. We therefore decided to use a linear model for all processing, as the quadratic model produced almost identical results and the cubic model produced unreliable results with poor spatial coverage. Both the Niyaqu and the Qugaqie basin are relatively stable in flat areas on a multiannual scale but show a strong seasonal signal in the same areas (Fig. 6A). It is unlikely that this signal is induced by seasonal atmospheric effects, as the amplitude would likely correlate to some degree with relative elevation to the reference points (Dong et al., 2019), which is not the case for our data. The most likely explanation is, that this signal displays the freeze-thaw cycle of moist soil. Others observed very similar signals over permafrost areas and seasonally frozen ground on the northern TP (Daout et al., 2017) and in Dangxiong county on the southern side of the Nyainqêntanglha range (Li et al., 2015). We estimated a sine function for every individual time series to determine the spatial distribution of this signal. This is only an approximation of this signal and not a true representation of its parameters as it does not follow the trend of a sine curve perfectly. Nonetheless we consider it a valid if imperfect approach. We could not identify any significant difference in the freeze-thaw cycle between areas where permafrost is likely to be present and areas where the ground is only seasonally frozen. We therefore disagree with similar studies (Daout et al, 2017; Li et al., 2015) that associated this process with permafrost. The amplitude, the day of maximum thaw subsidence and the active layer thickness of those studies agree well with our results from the Niyaqu basin. In the Qugaqie basin this is not the case for the latter two. Li et al. (2015) observe an increasing lag time of up to 98 days in mountainous areas, which they attributed to thicker permafrost and colder surroundings. A small amount of their data points fall within the Qugaqie basin, showing lag times of 50 to 90 days. We observe a significantly shorter lag time, with most areas in this basin reaching their maximum subsidence ahead of the maximum air temperature by a few days to weeks (Fig. 4). It is possible, that the difference between their results and ours is reflecting actual changes to the lag time between their dataset of 2007 to 2011 and ours of 2015 to 2018 but the point density of their data within Qugaqie basin is too low to draw reliable conclusions. The absence of a lag time in the Qugaqie basin in our results could possibly be explained by the small size of the basin. Its small size may let the basin react much quicker to environmental changes, such as dropping temperatures, compared to a larger basin like the Niyaqu. It is also possible, that the thawing process in the Qugaqie basin is not as closely linked to air temperature and other parameters, such as precipitation and glacial meltwater, play a larger role.



505 Most regions with small slopes throughout both basins can be considered relatively stable with mean
vertical and east-west velocities within $\pm 5 \text{ mm yr}^{-1}$. Some regions in valleys show uplift rates of up to
40 mm yr^{-1} (Qugaqie basin, Fig. 3B) and 21 mm yr^{-1} (Niyaqu basin, Fig. 3A). These regions are likely
experiencing some form of sediment accumulation through the nearby streams. We also observe
subsidence rates of up to -12 mm yr^{-1} in Qugaqie basin and -25 mm yr^{-1} in Niyaqu basin. Many of
510 those data points are close to streams or other water bodies, making fluvial processes the most likely
cause. However, approximately 30 % in the Niyaqu and 60 % in the Qugaqie basin fall into permafrost
regions (Zou et al., 2017; Tian et al., 2009) further away from water bodies. This makes permafrost
degradation a potential driver of this subsidence, as a thinning permafrost layer would result in
meltwater escaping from the thawing soil.

515 Most data points on slopes in both basins show downslope velocities of 8 to 17 mm yr^{-1} with a small
number of landforms moving faster than 50 mm yr^{-1} . The instability of most sloped areas is to be
expected, as there is very little deep-rooted vegetation to prevent the unconsolidated material from
sliding. Most soil covered slopes, especially in the Niyaqu basin, heavily feature *Kobresia pygmaea*
pastures, which forms a grass mat with a thick root system of up to 30 cm. This may provide some
stability in the absence of larger vegetation, however both climate change and overgrazing are
520 degrading this grass mat (Miehe et al., 2008), which could lead to larger sliding velocities in the
future. Most slopes moving at least 10 mm yr^{-1} experience a clear seasonal displacement signal, with
velocities increasing significantly during the summer monsoon period (Fig. 6C). Monsoon season is
associated with both the highest temperatures and approximately 80 % of the annual precipitation
over a period of 4 months from June to September (NAMORS, 2018). For Qugaqie basin it is also the
525 only time when the average daily air temperature exceeds 0°C (Zhang et al., 2013). Relatively warm
temperatures thaw the ground, likely accelerated by the increased thermal conductivity of moist soil
compared to dry soil (Li et al., 2015), which facilitates faster sliding during this period. Remarkably we
do not observe this seasonal velocity pattern for most of the fastest moving landforms like rock
glaciers. These landforms are sliding at very linear rates, without significant differences between
530 summer and winter (Fig. 6B), often with downslope velocities $> 50 \text{ mm yr}^{-1}$. We were able to identify
19 of these landforms in the Niyaqu basin and 32 in the Qugaqie basin by clustering data points with
a strong linear pattern and high slope velocities. Our spatial data coverage of steep slopes is better in
the Qugaqie basin compared to the Niyaqu basin. It is therefore unlikely that this 19 to 32
comparison is an accurate reflection of the difference in frequency of these landforms between both
535 study areas. We see it however as a strong indication of a landform relegated exclusively to
mountainous terrain. It is possible that some of these clusters have been misidentified as linearly
moving, while actually featuring both the seasonal freeze-thaw cycle prevalent in the valleys and the
seasonal sliding pattern of the slopes. In some cases those two cycles may cancel each other out to



540 such a degree that the resulting velocity appears linear. This can be observed at the interface
between slopes and the valley (Fig. 3C). We determined from optical satellite data, DEM analysis and
field observations, that some of these linearly creeping clusters are associated with rock glaciers or
other periglacial landforms, whose motion is driven by high ice content. It is therefore possible that
fast linear velocity is an indicator for ice-driven landforms. This disagrees with some other studies
observing strong seasonal variations in the velocities of rock glaciers (Kääb and Vollmer, 2000). Rock
545 glacier kinematics are highly dependent on the climatic setting, ice content, ground lithology and
slope (Haeberli et al., 2006), making comparison between rock glaciers of different regions difficult.
Rock glaciers studied in the Himalaya in north-western Bhutan (Dini et al., 2019) and in the Khumbu
Himalaya (Barsch and Jakob, 1998) show comparable rock glacier velocities of 18 to 35 and 100 to
200 mm yr⁻¹ respectively. However, Dini et al. (2019) did not project their data along the steepest
550 slope, which explains the lower values, and neither study analyzed the seasonal displacement
patterns of rock glaciers in their study area. We can therefore not be certain if fast linear motion is
indeed an indicator of ice-driven motion in our study areas or if the linearity of the motion is related
to other processes. Further field work of permafrost and subsurface ice distribution in Qugaqie basin
and neighboring regions is required to corroborate or disprove this hypothesis.

555

Conclusion

We observe clearly both multiannual and seasonal surface displacement patterns at lake Nam Co.
Most flat areas are relatively stable on a multiannual scale but show a strong seasonal pattern
induced by thawing of the active layer in spring and summer and its subsequent freezing in late
560 autumn and winter. This causes a vertical oscillation with an amplitude of 5 to 10 mm in most regions
with areas near water bodies showing a more pronounced pattern with an amplitude of up to 24
mm. We observe uplift rates of 10 to 40 mm yr⁻¹ in near some rivers, likely representing accumulation
of material, and subsidence rates of 10 to 20 mm yr⁻¹, which may be associated with permafrost
degradation. Slopes in both study areas are largely unstable, due to the unconsolidated material and
565 the lack of deep-rooted vegetation. They move downslope with velocities of 8 to 17 mm yr⁻¹. Most
slopes follow a seasonal sliding pattern, forced by the monsoonal climate, which brings both heavy
rainfall and warmer temperatures to an otherwise cold and dry region. Velocities may be up to one
magnitude larger in summer compared to winter, with some slopes in the Qugaqie basin arresting
almost all motion during the winter months. The fastest moving landforms can reach downslope
570 velocities of over 100 mm yr⁻¹. These landforms do not follow the seasonal sliding pattern of most
slopes but creep linearly with very little difference between summer and winter velocity. While we



have identified some of those landforms as rock glaciers and protalus ramparts, we cannot be certain if fast linear velocity is an indicator for ice-driven motion in this area. Further field work is necessary to corroborate or disprove this hypothesis.

575

Data availability

<https://doi.pangaea.de/10.1594/PANGAEA.907743>

Team List

580 M. Sc. Eike Reinosch, Institute of Geodesy and Photogrammetry, Technische Universität Braunschweig, 38106, Braunschweig, Germany, e.reinosch@tu-braunschweig.de, phone: +49 531 391 94587

M. Sc. Johannes Buckel, Institute of Geophysics and extraterrestrial Physics, Technische Universität Braunschweig, 38106, Braunschweig, Germany, j.buckel@tu-bs.de, phone: +49 531 391 8506

585 Dr. Jie Dong, School of Remote Sensing and Information Engineering, Wuhan University, 430079, Wuhan, China, dongjie@whu.edu.cn, phone: +86 15072317889

Prof. Markus Gerke, Institute of Geodesy and Photogrammetry, Technische Universität Braunschweig, 38106, Braunschweig, Germany, m.gerke@tu-bs.de, phone: +49 531 391 94570

590 Dr. Jussi Baade, Department of Geography, Friedrich-Schiller- Universität Jena, 07743, Jena, Germany, jussi.baade@uni-jena.de, phone: +49 3641 9-48803

Dr. Björn Riedel, Institute of Geodesy and Photogrammetry, Technische Universität Braunschweig, 38106, Braunschweig, Germany, b.riedel@tu-bs.de, phone: +49 531 391 94593

Author Contribution

595 The majority of the scientific writing and the figures were produced by Eike Reinosch. He also performed most of the literature research and data processing. Johannes Buckel performed literature research of the study areas, especially about their geomorphology, and wrote parts of the respective section. Furthermore he proof read the entire document regarding geomorphological and geological data and established connections between the results of the satellite analysis and relevant
600 geomorphological landforms and processes in the field. Dr. Björn Riedel provided guidance regarding



InSAR processing and proof reading of the manuscript, with a focus on the technical aspects of InSAR time series analysis. He also secured the funding for this research as part of the TransTiP project. Prof. Markus Gerke proof read the manuscript, provided guidance about the relevant research questions, research direction and the manuscript structure and aided in establishing connections to other remote sensing instituting to discuss the content of this research with fellow researchers. Dr. Jussi Baade secured funding for the project, evaluated potential study areas and provided us with additional data through additional proposals to the DLR. Dr. Jie Dong performed a review of the methods used with a focus on the seasonal displacement signal present in our data and the potential causes thereof.

610

Competing Interests

The authors declare that they have no conflict of interests.

Acknowledgements

615 We would like to thank the DLR for providing us with the high-resolution TanDEM-X DEM for our data processing (Proposal ID DEM_HYDR1727) and the ESA and Copernicus for making Sentinel-1 and Sentinel-2 data freely available to the public. We are especially grateful to the 'Deutsche Forschungsgemeinschaft' (DFG) for funding our work as part of the Sino-German project 'Geoecosystems in transition on the Tibetan Plateau' (TransTiP; GRK 2309/1). We thank our Chinese colleagues, who have worked tirelessly to support us before and during our field work.

620

References

- 625 Barsch, D. and Jakob, M.: Mass transport by active rockglaciers in the Khumbu Himalaya. *Geomorphology*, 26(1-3), 215-222, [https://doi.org/10.1016/S0169-555X\(98\)00060-9](https://doi.org/10.1016/S0169-555X(98)00060-9), 1998.
- Bateson, L., Cigna, F., Boon, D. and Sowter, A.: The application of the Intermittent SBAS (ISBAS) InSAR method to the South Wales Coalfield, UK. *International Journal of Applied Earth Observation and Geoinformation*, 34, 249-257, <https://doi.org/10.1016/j.jag.2014.08.018>, 2015.
- 630 Berardino, P., Fornaro, G., Lanari, R., and Sansosti, E.: A new algorithm for surface deformation monitoring based on small baseline differential SAR interferograms. *IEEE Transactions on geoscience and remote sensing*, 40(11), 2375-2383, <https://doi.org/10.1109/TGRS.2002.803792>, 2002



- 635 Bolch, T., Yao, T., Kang, S., Buchroithner, M. F., Scherer, D., Maussion, F., Huintjes, E., and Schneider, C.: A glacier inventory for the western Nyainqentanglha Range and the Nam Co Basin, Tibet, and glacier changes 1976–2009, *The Cryosphere*, 4, 419–433, <https://doi.org/10.5194/tc-4-419-2010>, 2010.
- 640 Crosetto, M., Monserrat, O., Cuevas-González, M., Devanthéry, N. and Crippa, B.: Persistent scatterer interferometry: A review. *ISPRS Journal of Photogrammetry and Remote Sensing*, 115, 78-89, <https://doi.org/10.1016/j.isprsjprs.2015.10.011>, 2016.
- 645 Daanen, R. P., Grosse, G., Darrow, M. M., Hamilton, T. D. and Jones, B. M.: Rapid movement of frozen debris-lobes: implications for permafrost degradation and slope instability in the south-central Brooks Range, Alaska. *Natural Hazards and Earth System Sciences*, 12(5), 1521-1537, <https://doi.org/10.5194/nhess-12-1521-2012>, 2012.
- 650 Daout, S., Doin, M. P., Peltzer, G., Socquet, A. and Lasserre, C.: Large-scale InSAR monitoring of permafrost freeze-thaw cycles on the Tibetan Plateau. *Geophysical Research Letters*, 44(2), 901-909, <https://doi.org/10.1002/2016GL070781>, 2017.
- 655 Dini, B., Manconi, A. and Loew, S.: Investigation of slope instabilities in NW Bhutan as derived from systematic DInSAR analyses. *Engineering Geology*, 259, 105111, <https://doi.org/10.1016/j.enggeo.2019.04.008>, 2019.
- 660 Dong, J., Zhang, L., Liao, M. and Gong, J.: Improved correction of seasonal tropospheric delay in InSAR observations for landslide deformation monitoring. *Remote Sensing of Environment*, 233, 111370, <https://doi.org/10.1016/j.rse.2019.111370>, 2019.
- 665 ESA (European Space Agency): SENTINEL-1. ESA's Radar Observatory Mission for GMES Operational Services, ESA SP-1322/1, Noordwijk, 2012.
- 670 Eriksen, H. Ø., Lauknes, T. R., Larsen, Y., Corner, G. D., Bergh, S. G., Dehls, J. and Kierulf, H. P.: Visualizing and interpreting surface displacement patterns on unstable slopes using multi-geometry satellite SAR interferometry (2D InSAR). *Remote Sensing of Environment*, 191, 297-312, <https://doi.org/10.1016/j.rse.2016.12.024>, 2017.
- 675 Haerberli, W., Hallet, B., Arenson, L., Elconin, R., Humlum, O., Kääh, A., Kaufmann, V., Ladanyi, B., Matsuoka, N., Springmann, S. and Mühl, D. V.: Permafrost creep and rock glacier dynamics. *Permafrost and Periglacial Processes*, 17(3), 189-214, <https://doi.org/10.1002/ppp.561>, 2006.
- Jarvis, A., Reuter, H. I., Nelson, A. and Guevara, E.: Hole-filled SRTM for the globe Version 4, International Centre for Tropical Agriculture (CIAT), available from <http://srtm.csi.cgiar.org>, 2008.
- Jiang, L., Nielsen, K., Andersen, O. B. and Bauer-Gottwein, P.: Monitoring recent lake level variations on the Tibetan Plateau using CryoSat-2 SARIn mode data. *Journal of Hydrology*, 544, 109-124, <https://doi.org/10.1016/j.jhydrol.2016.11.024>, 2017.



- 680 Jones, D. B., Harrison, S., Anderson, K. and Whalley, W. B.: Rock glaciers and mountain hydrology: A review. *Earth-Science Reviews*, <https://doi.org/10.1016/j.earscirev.2019.04.001>, 2019.
- Keil, A., Berking, J., Mügler, I., Schütt, B., Schwalb, A. and Steeb, P.: Hydrological and geomorphological basin and catchment characteristics of Lake Nam Co, South-Central Tibet. *Quaternary International*, 218(1-2), 118-130, <https://doi.org/10.1016/j.quaint.2009.02.022>, 2010.
- 685 Kropáček, J., Braun, A., Kang, S., Feng, C., Ye, Q. and Hochschild, V.: Analysis of lake level changes in Nam Co in central Tibet utilizing synergistic satellite altimetry and optical imagery. *International Journal of Applied Earth Observation and Geoinformation*, 17, 3-11, <https://doi.org/10.1016/j.jag.2011.10.001>, 2012.
- 690 Lei, Y., Yao, T., Bird, B. W., Yang, K., Zhai, J. and Sheng, Y.: Coherent lake growth on the central Tibetan Plateau since the 1970s: Characterization and attribution. *Journal of Hydrology*, 483, 61-67, <https://doi.org/10.1016/j.jhydrol.2013.01.003>, 2013.
- 695 Li, Z. W., Xu, W. B., Feng, G. C., Hu, J., Wang, C. C., Ding, X. L. and Zhu, J. J.: Correcting atmospheric effects on InSAR with MERIS water vapour data and elevation-dependent interpolation model. *Geophysical Journal International*, 189(2), 898-910, <https://doi.org/10.1111/j.1365-246X.2012.05432.x>, 2012.
- 700 Li, B., Yu, Z., Liang, Z. and Acharya, K.: Hydrologic response of a high altitude glacierized basin in the central Tibetan Plateau. *Global and Planetary Change*, 118, 69-84, <https://doi.org/10.1016/j.gloplacha.2014.04.006>, 2014.
- 705 Li, Z., Zhao, R., Hu, J., Wen, L., Feng, G., Zhang, Z. and Wang, Q.: InSAR analysis of surface deformation over permafrost to estimate active layer thickness based on one-dimensional heat transfer model of soils. *Scientific Reports*, 5, 15542, <https://doi.org/10.1038/srep15542>, 2015.
- 710 Li, Q.: Spatial variability and long-term change in pollen diversity in Nam Co catchment (central Tibetan Plateau): Implications for alpine vegetation restoration from a paleoecological perspective. *Science China Earth Sciences*, 61(3), 270-284, <https://doi.org/10.1007/s11430-017-9133-0>, 2018.
- Liu, L., Millar, C. I., Westfall, R. D. and Zebker, H.: Surface motion of active rock glaciers in the Sierra Nevada, California, USA: inventory and a case study using InSAR. *The Cryosphere*. 7: 1109-1119, 7, 1109-1119, <https://doi.org/10.5194/tc-7-1109-2013>, 2013.
- 715 Messerli, B., Viviroli, D., and Weingartner, R.: Mountains of the World: Vulnerable Water Towers for the 21st Century. *AMBIO*, 2004, 29-3, 2004.
- 720 Mieke, G., Mieke, S., Kaiser, K., Jianquan, L. and Zhao, X.: Status and dynamics of the Kobresia pygmaea ecosystem on the Tibetan Plateau. *AMBIO: A Journal of the Human Environment*, 37(4), 272-280, [https://doi.org/10.1579/0044-7447\(2008\)37\[272:SADOTK\]2.0.CO;2](https://doi.org/10.1579/0044-7447(2008)37[272:SADOTK]2.0.CO;2), 2008.



- 725 Mügler, I., Gleixner, G., Günther, F., Mäusbacher, R., Daut, G., Schütt, B., Berking, J., Schwalb, A., Schwark, L., Xu, B., Yao, T., Zhu, L. and Yi, C.: A multi-proxy approach to reconstruct hydrological changes and Holocene climate development of Nam Co, Central Tibet. *Journal of Paleolimnology*, 43(4), 625-648, <https://doi.org/10.1007/s10933-009-9357-0>, 2010.
- NAMORS 2018: Meteorological Data for the NAMORS research station, 2010 to 2017. ITP – CAS Lhasa
- 730 Notti, D., Herrera, G., Bianchini, S., Meisina, C., García-Davalillo, J. C. and Zucca, F.: A methodology for improving landslide PSI data analysis. *International Journal of Remote Sensing*, 35(6), 2186-2214, <https://doi.org/10.1080/01431161.2014.889864>, 2014.
- Osmanoğlu, B., Sunar, F., Wdowinski, S. and Cabral-Cano, E.: Time series analysis of InSAR data: Methods and trends. *ISPRS Journal of Photogrammetry and Remote Sensing*, 115, 90-102, 735 <https://doi.org/10.1016/j.isprsjprs.2015.10.003>, 2016.
- Sowter, A., Bateson, L., Strange, P., Ambrose, K. and Syafiudin, M. F.: DInSAR estimation of land motion using intermittent coherence with application to the South Derbyshire and Leicestershire coalfields. *Remote Sensing Letters*, 4(10), 979-987, <https://doi.org/10.1080/2150704X.2013.823673>, 740 2013.
- Tian, K., Liu, J., Kang, S., Campbell, I. B., Zhang, F., Zhang, Q. and Lu, W.: Hydrothermal pattern of frozen soil in Nam Co lake basin, the Tibetan Plateau. *Environmental Geology*, 57(8), 1775-1784, <https://doi.org/10.1007/s00254-008-1462-2>, 2009. 745
- Wang, K., Wang, P., Liu, J., Sparrow, M., Haginoya, S. and Zhou, X. (2005). Variation of surface albedo and soil thermal parameters with soil moisture content at a semi-desert site on the western Tibetan Plateau. *Boundary-Layer Meteorology*, 116(1), 117-129, <https://doi.org/10.1007/s10546-004-7403-z>, 2005. 750
- Wang, X., Liu, L., Zhao, L., Wu, T., Li, Z., and Liu, G.: Mapping and inventorying active rock glaciers in the northern Tien Shan of China using satellite SAR interferometry, *The Cryosphere*, 11, 997–1014, <https://doi.org/10.5194/tc-11-997-2017>, 2017.
- 755 Wessel, B., Huber, M., Christian Wohlfart, C., Ursula Marschalk, U., Detlev Kosmann, D., and Achim Roth, A.: Accuracy assessment of the global TanDEM-X Digital Elevation Model with GPS data, *ISPRS Journal of Photogrammetry and Remote Sensing*, 139, 171-182, <https://doi.org/10.1016/j.isprsjprs.2018.02.017>, 2018.
- 760 Wu, Q., Zhang, T. and Liu, Y.: Permafrost temperatures and thickness on the Qinghai-Tibet Plateau. *Global and Planetary Change*, 72(1-2), 32-38, <https://doi.org/10.1016/j.gloplacha.2010.03.001>, 2010.



- 765 Yagüe-Martínez, N., Prats-Iraola, P., Gonzalez, F. R., Brcic, R., Shau, R., Geudtner, D., Eineder, M. and Bamler, R.: Interferometric processing of Sentinel-1 TOPS data. *IEEE Transactions on Geoscience and Remote Sensing*, 54(4), 2220-2234, <https://doi.org/10.1109/TGRS.2015.2497902>, 2016.
- Yao, T., Liu, X., Wang, N. and Shi, Y.: Amplitude of climatic changes in Qinghai-Tibetan Plateau. *Chinese Science Bulletin*, 45(13), 1236-1243, <https://doi.org/10.1007/BF02886087>, 2000.
- 770 Yao, T., Pu, J., Lu, A., Wang, Y. and Yu, W.: Recent glacial retreat and its impact on hydrological processes on the Tibetan Plateau, China, and surrounding regions. *Arctic, Antarctic, and Alpine Research*, 39(4), 642-650, [https://doi.org/10.1657/1523-0430\(07-510\)\[YAO\]2.0.CO;2](https://doi.org/10.1657/1523-0430(07-510)[YAO]2.0.CO;2), 2007.
- 775 Yao, T., Masson-Delmotte, V., Gao, J., Yu, W., Yang, X., Risi, C., Sturm, C., Werner, M., Zhao, H., He, Y., Ren, W., Tian, L., Shi, C. and Hou, S.: A review of climatic controls on $\delta^{18}\text{O}$ in precipitation over the Tibetan Plateau: Observations and simulations. *Reviews of Geophysics*, 51(4), 525-548, <https://doi.org/10.1002/rog.20023>, 2013.
- 780 Ye, Q., Zong, J., Tian, L., Cogley, J. G., Song, C. and Guo, W.: Glacier changes on the Tibetan Plateau derived from Landsat imagery: mid-1970s–2000–13. *Journal of Glaciology*, 63(238), 273-287, <https://doi.org/10.1017/jog.2016.137>, 2017.
- 785 Zhang, G., Kang, S., Fujita, K., Huintjes, E., Xu, J., Yamazaki, T., Haginoya, S., Wei, Y., Scherer, D., Schneider, C. and Yao, T.: Energy and mass balance of Zhadang glacier surface, central Tibetan Plateau. *Journal of Glaciology*, 59(213), 137-148, <https://doi.org/10.3189/2013JoG12J152>, 2013.
- 790 Zhang, G., Li, J. and Zheng, G.: Lake-area mapping in the Tibetan Plateau: an evaluation of data and methods. *International Journal of Remote Sensing*, 38(3), 742-772, <https://doi.org/10.1080/01431161.2016.1271478>, 2017.
- 795 Zhao, R., Li, Z. W., Feng, G. C., Wang, Q. J. and Hu, J.: Monitoring surface deformation over permafrost with an improved SBAS-InSAR algorithm: With emphasis on climatic factors modeling. *Remote Sensing of Environment*, 184, 276-287, <https://doi.org/10.1016/j.rse.2016.07.019>, 2016.
- Zhou, S., Kang, S., Chen, F. and Joswiak, D. R.: Water balance observations reveal significant subsurface water seepage from Lake Nam Co, south-central Tibetan Plateau. *Journal of Hydrology*, 491, 89-99, <https://doi.org/10.1016/j.jhydrol.2013.03.030>, 2013.
- 800 Zink, M., Bachmann, M., Bräutigam, B., Fritz, T., Hajnsek, I., Moreira, A., Wessel, B., and Krieger, G.: TanDEM-X: The New Global DEM Takes Shape, *IEEE Geoscience and Remote Sensing Magazine*, 2(2), 8–23, <https://doi.org/10.1109/MGRS.2014.2318895>, 2014.

<https://doi.org/10.5194/tc-2019-262>

Preprint. Discussion started: 11 December 2019

© Author(s) 2019. CC BY 4.0 License.



805 Zou, D., Zhao, L., Yu, S., Chen, J., Hu, G., Wu, T., Wu, J., Xie, C., Wu, X., Pang, Q., Wang, W., Du, E., Li, W., Liu, G., Li, J., Qin, Y., Qiao, Y., Wang, Z., Shi, J. and Cheng, G.: A new map of permafrost distribution on the Tibetan Plateau. *The Cryosphere*, 11(6), 2527, <https://doi.org/10.5194/tc-11-2527-2017>, 2017.